

## PLAQUE PROGRESSION MODELING BY USING COMPUTER SIMULATION AND IMAGING DATA

Nenad Filipovic<sup>1\*</sup>, Dalibor Nikolic<sup>1</sup>, Zarko Milosevic<sup>1</sup>, Milos Radovic<sup>1</sup>, Igor Saveljic<sup>1</sup>, Themis Exarcous<sup>2</sup>, Dimitris Fotiadis<sup>2</sup>, Walter Pelosi<sup>3</sup> and Oberdan Parodi<sup>3</sup>

<sup>1</sup>University of Kragujevac, Kragujevac, Serbia, [fica@kg.ac.rs](mailto:fica@kg.ac.rs)

<sup>2</sup>University of Ioannina, Ioannina, Greece, [dimitris.fotiadis30@gmail.com](mailto:dimitris.fotiadis30@gmail.com)

<sup>3</sup>CNR Clinical Physiology Institute, Pisa, Italy, [oberpar@tin.it](mailto:oberpar@tin.it)

\*) Corresponding author

### ABSTRACT

Atherosclerosis is a progressive disease characterized by inflammation, monocyte-macrophage migration, and lipid accumulation in the vascular wall. In this study, two experiments are calculated numerically. The first is Cheng et al 2006 experiment with cast model on the carotid artery and the second is our pig experiment on the left anterior descending coronary artery (LAD) after 2 month of high fat diet. Experimental model of plaque formation on pig LAD is simulated numerically using a specific animal data obtained from intravascular ultrasound (IVUS) and histological data. The 3D blood flow is governed by the Navier-Stokes equations, together with the continuity equation. Mass transfer within the blood lumen and through the arterial wall is coupled with the blood flow and is modeled by the convection-diffusion equation. LDL transport in lumen of the vessel is described by Kedem-Katchalsky equations. The inflammatory process is solved using three additional reaction-diffusion partial differential equations. Matching of IVUS and histological animal data is performed using 3D histological image reconstruction and 3D deformation of elastic body. Lipids concentration in the intimal area of the low shear stress was 16% and for oscillatory zone 10% which is in good agreement with experimental data. Matching of plaque location and progression in time between experimental and computer model shows a potential benefit for future prediction of this vascular disease using computer simulation.

### KEY WORDS

Finite Element Model (FEM), Computer Fluid Dynamic (CFD), Atherosclerosis, Wall Shear Stress, LDL, Lipid Accumulation, Plaque.

### 1. Introduction

Atherosclerosis is a disease of the large arteries characterized by the blood vessel endothelial dysfunction and lipid, cholesterol, calcium and cell elements accumulations inside blood vessel wall [1]. It is commonly referred as plaque formation, vascular remodeling, acute and chronic obstruction of blood vessel lumen, blood flow disorder and lower oxygenation of relevant tissues. Many studies confirmed different risk factor which contributes development and spreading of the atherosclerosis, the most common are hyperlipidemia, higher blood pressure and sugar values, cigarette consumption, age and sex. Great contribution to atherosclerosis development gives mechanical quantities such as low shear stress areas which causes endothelium dysfunctions and arterogenesis [2]. The main objective of this study is to examine influence of low shear stress and arterial mass transport by modeling the blood flow and solution transport processes in arterial lumen and the wall. Transport processes of the atherogenic species such as low density lipoprotein (LDL) from the bulk blood flow to and across arterial wall contributes to lipid accumulation in the wall [2].

Several mathematical models have recently been set up for the transport of macromolecules, such as low-density lipoproteins, from the arterial lumen to the arterial wall and inside the wall [3-5]. These models are usually classified in three categories according to the level of description of the arterial wall. The simplest model is called the wall-free model, since in this model the arterial wall is simply described by means of an appropriate boundary condition. Kaazempur-Mofrad and Ethier [6] simulated the mass transport in a realistic human right coronary artery and Wada et al [7] used a wall-free model to study the concentration polarization phenomenon. The wall-free model does not provide any information on the transmural flow and solute dynamics in the arterial wall.

The fluid-wall models that can be either single-layer or multilayer account for the solute dynamics not only in the lumen, but also in the arterial wall. Stangeby and Ethier [8] analysed the wall as single layer porous medium and solved the coupled luminal blood flow and transmural fluid flow using Brinkman's equations. Sun et al [9] used single and Al and Vafai [10] used multilayer models which represent intima and media separately. Olgac et al [11] used a three-pore model for LDL transport.

It is now well known that the early stage of the inflammatory disease is the result of interaction between plasma low density lipoproteins that filtrate through endothelium into the intima, cellular components (monocytes/macrophages, endothelial cells and smooth muscle cells) and the extracellular matrix of the arterial wall [1],[12].

In this study we performed computational study for plaque composition and initial progression. The aim is to connect LDL transport with macrophages and oxidized LDL distribution as well as initial plaque grow model inside the intimal area. We firstly described mass transport of LDL through the wall and the simplified inflammatory process. The Navier-Stokes equations govern the blood motion in the lumen, the Darcy law is used for model blood filtration, Kedem-Katchalsky equations [13-14] for the solute and flux exchanges between the lumen and the intima. Then we described the system of three additional reaction-diffusion equations that models the inflammatory process and lesion growth model in the intima. This model relies on a matter incompressibility assumption. The next sections are devoted to numerical simulation examples in two and three dimension domain and comparison with experimental results from literature and our own experimental data.

## 2. Methods

The fundamental equations for the LDL transport through blood vessel lumen and wall, and for plaque development are given. Also procedure for estimation of plaque growth function is described. The three-dimensional blood flow in lumen domain is modeled by the Navier-Stokes equations, together with the continuity equation of incompressible fluid:

$$-\mu\nabla^2\mathbf{u}_l + \rho(\mathbf{u}_l \cdot \nabla)\mathbf{u}_l + \nabla p_l = 0 \quad (1)$$

$$\nabla \cdot \mathbf{u}_l = 0 \quad (2)$$

where  $\mathbf{u}_l$  is blood velocity in the lumen,  $p_l$  is pressure,  $\mu$  is the dynamic viscosity of blood, and  $\rho$  is blood density [15].

Mass transfer in the blood lumen is coupled with the blood flow by a convection-diffusion equation,

$$\nabla \cdot (-D_l \nabla c_l + c_l \mathbf{u}_l) = 0 \quad (3)$$

in the fluid domain, where  $c_l$  is the solute concentration in the blood lumen, and  $D_l$  is the solute diffusivity in the lumen. Mass transfer in the arterial wall is coupled to the transmural flow and modeled by a convection-diffusion-reaction equation as follows

$$\nabla \cdot (-D_w \nabla c_w + K c_w \mathbf{u}_w) = r_w c_w \quad (4)$$

where  $c_w$  is the solute concentration and  $D_w$  is the solute diffusivity in the arterial wall;  $\mathbf{u}_w$  is blood velocity in the wall,  $K$  is the solute lag coefficient, and  $r_w$  is the consumption rate constant. The LDL transports in lumen and in the vessel wall are coupled by the Kedem-Katchalsky equations:

$$J_v = L_p (\Delta p - \sigma_d \Delta \pi) \quad (5)$$

$$J_s = P \Delta c + (1 - \sigma_f) J_v \bar{c} \quad (6)$$

where  $L_p$  is hydraulic conductivity of the endothelium;  $\Delta c$  is the solute concentration difference,  $\Delta p$  is the pressure drop and  $\Delta \pi$  is the oncotic pressure difference, all across the endothelium;  $\sigma_d$  is the osmotic reflection coefficient,  $\sigma_f$  is the solvent reflection coefficient,  $P$  is the solute endothelial permeability, and  $\bar{c}$  is the mean endothelial concentration. The first term in Kedem-Katchalsky equations  $P \Delta c$  of the right hand side in (Eq 6) defines the diffusive flux across the endothelium, while the second term  $(1 - \sigma_f) J_v \bar{c}$  defines the convective flux. Only the oncotic pressure difference  $\Delta \pi$  is neglected in our simulations because of decoupling the fluid dynamics from solute dynamics.

The above governing equations are transformed into a finite element system of incremental-iterative equations and solved over time steps.

The atherosclerotic process starts with the accumulation of LDL in the intima, where part of them are oxidized and become pathological. In order to remove the oxidized particles, circulating immune cells (*e.g.* monocytes) are recruited. Once in the intima, the monocytes differentiate and become macrophages that phagocyte the oxidized LDL. Fatty macrophages then transform into foam cells. Foam cells are responsible for the growth of a subendothelial plaque which eventually emerges in the artery lumen.

The inflammatory process is modeled using three additional reaction-diffusion partial differential equations [16],[17],[18]:

$$\begin{aligned} \partial_t O &= d_1 \Delta O - k_1 O \cdot M \\ \partial_t M + \text{div}(v_w M) &= d_2 \Delta M - k_1 O \cdot M + S / (1 + S) \\ \partial_t S &= d_3 \Delta S - \lambda S + k_1 O \cdot M + \gamma(O - O^{thr}) \end{aligned} \quad (7)$$

where  $O$  is the oxidized LDL in the wall,  $M$  and  $S$  are concentrations in the intima of macrophages and

cytokines, respectively;  $d_1, d_2, d_3$  are the corresponding diffusion coefficients;  $\lambda$  and  $\gamma$  are degradation and LDL oxidized detection coefficients; and  $v_w$  is the inflammatory velocity of plaque growth, which satisfies Darcy's law and incompressibility continuity equation [18]:

$$v_w - \nabla \cdot (p_w) = k_1 O \cdot M \quad (8)$$

$$\nabla v_w = 0 \quad (9)$$

in the wall domain. Here,  $p_w$  is the pressure in the arterial wall.

In order to follow change of the vessel wall geometry during plaque growth, a 3D mesh moving algorithm ALE (Arbitrary Lagrangian Eulerian) is applied [19].

### 2.1 Mesh moving algorithm

The governing equations, which include the Navier-Stokes equations of balance of linear momentum and the continuity equation, can be written in the ALE formulation as [19].

$$\rho [v_i^* + (v_j - v_j^m) v_{i,j}] = -p_{,i} + \mu v_{i,jj} + f_i^B \quad (10)$$

$$v_{i,i} = 0 \quad (11)$$

where  $v_i$  and  $v_i^m$  are the velocity components of a generic fluid particle and of the point on the moving mesh occupied by the fluid particle, respectively;  $\rho$  is fluid density,  $p$  is fluid pressure,  $\mu$  is dynamic viscosity, and  $f_i^B$  are the body force components. The symbol “\*” denotes the mesh-referential time derivative, i.e. the time derivative at a considered point on the mesh,

$$(\ )^* = \frac{\partial(\ )}{\partial t} \Big|_{\xi_i = \text{const}} \quad (12)$$

and the symbol “ $_{,i}$ ” denotes partial derivative, i.e.

$$(\ )_{,i} = \frac{\partial(\ )}{\partial x_i} \quad (13)$$

We use  $x_i$  and  $\xi_i$  as Cartesian coordinates of a generic particle in space and of the corresponding point on the mesh, respectively. The repeated index means summation, from 1 to 3, i.e.  $j=1,2,3$  in Eq. (10), and  $i=1,2,3$  in Eq. (11). In deriving Eq. (10) we used the following expression for the material derivative (corresponding to a fixed material point)  $D(\rho v_i) / Dt$ ,

$$\frac{D(\rho v_i)}{Dt} = \frac{\partial(\rho v_i)}{\partial t} \Big|_{\xi} + (v_j - v_j^m) \frac{\partial(\rho v_j)}{\partial x_i} \quad (14)$$

The derivatives on the right-hand side correspond to a generic point on the mesh, with the mesh-referential derivative and the convective term.

Using the linearization (14) we obtain from (10) and (11) the system of ordinary differential equations in the form

$${}^t \mathbf{M}_{(1)} \mathbf{V}^* + {}^t \mathbf{K}_{(1),vw} \Delta \mathbf{V} + {}^t \mathbf{K}_{vp} \Delta \mathbf{P} = {}^{t+\Delta t} \mathbf{F}_{(1)} - {}^t \mathbf{F}_{(1)} \quad (15)$$

and

$${}^t \mathbf{M}_{(2)} \mathbf{V}^* + {}^t \mathbf{K}_{(2),vw} \Delta \mathbf{V} = {}^{t+\Delta t} \mathbf{F}_{(2)} - {}^t \mathbf{F}_{(2)} \quad (16)$$

The matrices and vectors follow from the volume and surface integrals given in [19].

### 2.2 Fluid-structure interaction

For fluid-structure interaction problem the wall displacements can be large, hence the problem becomes geometrically nonlinear. Also, the tissue of blood vessels has nonlinear constitutive laws, leading to materially-nonlinear finite element formulation. For a nonlinear wall tissue problem, the incremental-iterative equation is using:

$${}^{n+1} \hat{\mathbf{K}}_{tissue}^{(i-1)} \Delta \mathbf{U}^{(i)} = {}^{n+1} \hat{\mathbf{F}}^{(i-1)} - {}^{n+1} \mathbf{F}^{\text{int}(i-1)} \quad (17)$$

where  $\Delta \mathbf{U}^{(i)}$  are the nodal displacement increments for the iteration ‘ $i$ ’, and the system matrix  ${}^{n+1} \hat{\mathbf{K}}_{tissue}^{(i-1)}$ , the force vector  ${}^{n+1} \hat{\mathbf{F}}^{(i-1)}$  and the vector of internal forces  ${}^{n+1} \mathbf{F}^{\text{int}(i-1)}$  correspond to the previous iteration. The geometrically linear part of the stiffness matrix,  $({}^{n+1} \mathbf{K}_L)_{tissue}^{(i-1)}$ , and nodal force vector,  ${}^{n+1} \mathbf{F}^{\text{int}(i-1)}$ , are defined:

$$\begin{aligned} ({}^{n+1} \mathbf{K}_L)_{tissue}^{(i-1)} &= \int_V \mathbf{B}_L^T {}^{n+1} \mathbf{C}_{tissue}^{(i-1)} \mathbf{B}_L dV \\ ({}^{n+1} \mathbf{F}^{\text{int}})^{(i-1)} &= \int_V \mathbf{B}_L^T {}^{n+1} \boldsymbol{\sigma}^{(i-1)} dV \end{aligned} \quad (18)$$

where the consistent tangent constitutive matrix  ${}^{n+1} \mathbf{C}_{tissue}^{(i-1)}$  of tissue and the stresses at the end of time step  ${}^{n+1} \boldsymbol{\sigma}^{(i-1)}$  depend on the material model used. Calculation of the matrix  ${}^{n+1} \mathbf{C}_{tissue}^{(i-1)}$  and the stresses  ${}^{n+1} \boldsymbol{\sigma}^{(i-1)}$  for the tissue material models are performed at each iteration.

The overall strategy of fluid-structure interaction adopted here consists of the following steps [15]:

- For the current geometry of the blood vessel, determine blood flow (with use of the ALE formulation when the wall displacements are large). Wall velocities at the common blood – blood vessel surface are taken as the boundary condition for the fluid.
- Calculate the loads, arising from the blood, which act on the walls.
- Determine deformation of the walls taking the current loads from the blood.
- Check for the overall convergence which includes fluid and solid. If convergence is reached, go to the next time step. Otherwise go to step a).
- Update blood domain geometry and velocities at the common solid-fluid boundary for the new calculation of the blood flow. In case of large wall displacements, update the FE mesh for the blood flow domain. Go to step a).

### 3. Results

#### 3.1 Simulation of plaque formation on experimental cast design in vivo

We validated firstly the initiation plaque model by reproducing Cheng *et al.* 2006 experiment [20]. This experiment that was run on mice confirms that lesions occur in preferred locations such as bends and bifurcations and that their biochemical composition may depend on the location. In these experiments, the arterial geometry has been modified by a perivascular cast that induces regions of lowered, increased, and lowered/oscillatory (i.e., with vortices) shear stresses (depicted in Figure 1). Mice are fed by a rich cholesterol diet in order to assess plaque formation and composition. Our aim was to obtain numerical results that fit with the experiments. We present the evolution and composition within our numerical simulations of the atherosclerotic plaque.

A fully developed parabolic steady velocity profile was assumed at the lumen inlet boundary

$$u(r) = 2U_0 \left( 1 - \left( \frac{2r}{D} \right)^2 \right) \quad (19)$$

where  $u(r)$  is the velocity in the axial direction at radial position  $r$ , and  $U_0 = 0.24 \text{ m/s}$  is the mean inlet velocity. The inlet artery diameter  $d_0 = 0.0004 \text{ [m]}$ . Blood was modeled as a Newtonian fluid with density  $\rho = 1050 \text{ [kg/m}^3 \text{]}$  and viscosity  $\mu = 0.0334 \text{ [P]}$ . The entering blood velocity is defined by the Reynolds number  $Re$  (calculated using the mean coronary blood velocity and the artery diameter). Basic values for this computer model are given in Table 1. Table 1. Values used for computational analysis for Cheng experiment

Lumen	Intima	Inflammation
$\rho = 1050 \text{ kg/m}^3$	$D_w = 1.3 \times 10^{-11} \text{ m}^2/\text{s}$	$d_1 = 10^{-7} \text{ m}^2/\text{s}$
$\mu = 0.0334 \text{ [P]}$	$r_w = -1.4 \times 10^{-4}$	$d_2 = 10^{-9} \text{ m}^2/\text{s}$
$D_1 = 2.8 \times 10^{-11} \text{ m}^2/\text{s}$	$P_{med} = 100 \text{ mmHg}$	$d_3 = 10^{-7} \text{ m}^2/\text{s}$
$U_{max} = 0.24 \text{ m/s}$		$k_1 = 10^{-6} \text{ m}^3/\text{kg s}$
$P_{out} = 100 \text{ mmHg}$		$\lambda = 20 \text{ s}^{-1}$
$C_0 = 2.86 \times 10^{-12} \text{ kg/m}^3$		$\gamma = 1 \text{ s}^{-1}$

The plaque initiation model provides oxidized LDL, macrophages and foam cells concentrations. Two dimensional asymmetric model is firstly implemented. The results for oxidized LDL, cytokines, macrophages and total wall LDL concentration distribution are presented in Figure 2. All the units are dimensionless respect to the input concentration  $C_0 = 2.86 \times 10^{-12} \text{ kg/m}^3$  (Tarbell 2003, [3]). It can be seen that for steady state condition low wall shear stress (WSS) appears after the cast which gives more LDL deposition in the recirculation zone. For two-dimensional model we use wall permeability function  $P$  of the WSS from eq. 6 where low WSS corresponds to the higher wall permeability. In three-dimensional model we found macrophages distributions in both zones of low WSS and recirculation WSS where

more oxidized LDL distribution is found in the zone of low WSS which corresponds to plaque composition of Cheng measurement (Figure 3). Here the permeability wall function depended from residence time of solutes in the neighborhood of vascular endothelium and oscillatory shear index (OSI). Also the artery/lumen shape is corresponding to Cheng experiment (Cheng et al, 2006 [20]). Quantification of macrophages and lipids in the intimal area of the lowered and oscillatory shear stress region from experiments and computational data are given in Table 1.

Table 1. Experimental data (exp) and computational results (comp) for macrophages and lipids in the intimal area at different shear stress for Cheng experiment

	Macrophages (area of % intima)	Lipids (area of % intima)
Low shear stress (exp)	28	16
Oscillatory shear stress (exp)	26	10
Low shear stress (comp)	27.3	16.2
Oscillatory shear stress (comp)	25.6	10.1

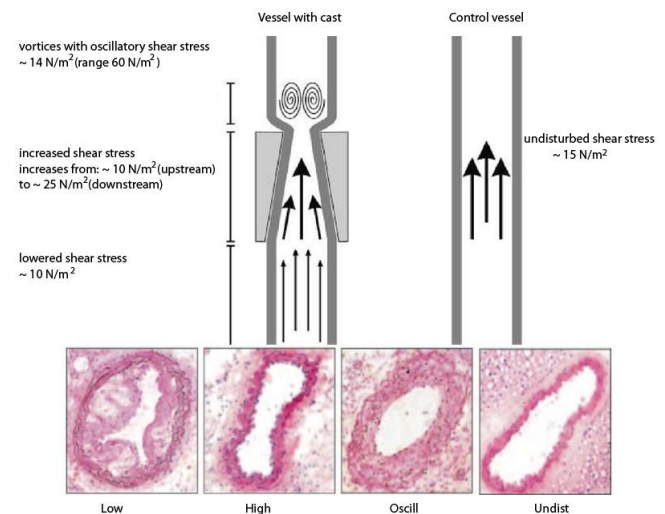


Figure 1. A mouse carotid vessel is partially obstructed with a cast. This modifies the blood flow, and particularly the WSS patterns. The growth of atheromatous plaques is correlated with the reduction of WSS (right before and after the cast). Moreover the composition of the plaques turn out to depend upon the WSS pattern: plaques associated with low WSS contain more oxidised LDL, whereas plaques located in zone of recirculating flow (after the cast) contain less oxidised LDL, (adapted from Cheng et al, 2006 [20])

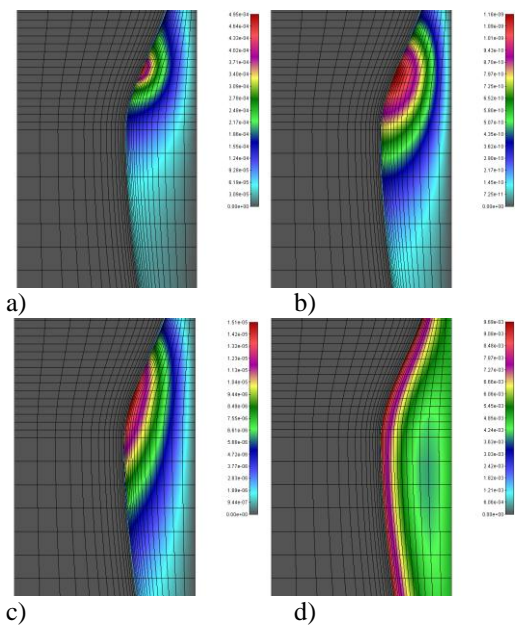


Figure 2. 2D asymmetric results for proximal to the cast position in the lowered shear stress zone. a) Oxidized LDL b) Cytokines c) Macrophages d) Total wall LDL concentration distribution. All units are dimensionless  $C/Co$ ,  $Co = 3 \times 10^{-12} \text{ kg/m}^3$

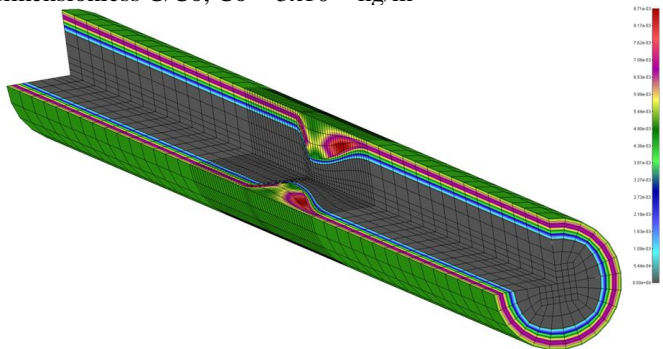


Figure 3. Oxidized LDL distribution for 3D Cheng experiment

### 3.2 Comparison with animal pig experiment on LAD induced atherosclerosis

For the second example we used data provided by the CNR Pisa, Italy in ARTreat project ([www.artreat.org](http://www.artreat.org)) on pigs submitted to a high cholesterol diet for two months. Specific software for 3D reconstruction of lumen domain and wall artery (coronary artery) was developed. Matching of histological data and IVUS slices is presented in Figure 4. A 3D reconstruction was done using standard IVUS and angiography images. After that, full three-dimensional finite element analysis was performed using our in-house finite element code (Filipovic et al 2010 [18]) in order to find low and oscillatory WSS zones. The LAD was used for this analysis. The process of matching with IVUS images was done by 2D deformation of each cross-section from histological analysis in order to keep the internal lumen length from IVUS images (Figure 5). The biggest plaque formation was found at 15 mm below LAD bifurcation

from left circumflex artery, which corresponds to low WSS zone. The volume of the plaque from histological analysis was fitted with specific nonlinear least square analysis in order to find parameters after 2 months of high fat diet for plaque formation and progression equations described in section 2. The fitted parameters are given in Table 2. Plaque size of 8% from intimal area was found at this location.

Macrophage concentration before and after 2 months of the high fat diet on the LAD 15 mm below bifurcation have been shown in Figure 6.

Table 2. Values for animal experiment

Lumen	Intima	Inflammation
$\rho = 1000 \text{ kg/m}^3$	$D_w = 1.3 \times 10^{-11} \text{ m}^2/\text{s}$	$d_1 = 10^{-8} \text{ m}^2/\text{s}$
$\mu = 0.035 [P]$	$r_w = -2.6 \times 10^{-4}$	$d_2 = 10^{-10} \text{ m}^2/\text{s}$
$D_1 = 1 \times 10^{-8} \text{ m}^2/\text{s}$	$P_{med} = 100 \text{ mmHg}$	$d_3 = 10^{-7} \text{ m}^2/\text{s}$
$U_{max} = 0.4 \text{ m/s}$		$k_1 = 10^{-6} \text{ m}^3/\text{kg s}$
$P_{out} = 110 \text{ mmHg}$		$\lambda = 25 \text{ s}^{-1}$
$Co = 3.0 \times 10^{-12} \text{ kg/m}^3$		$\gamma = 1 \text{ s}^{-1}$

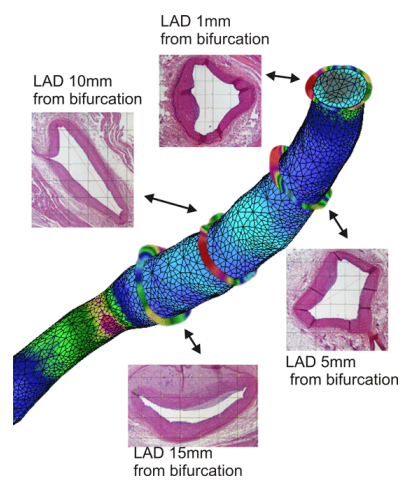


Figure 4. Matching IVUS and histological data with 3D computer simulation



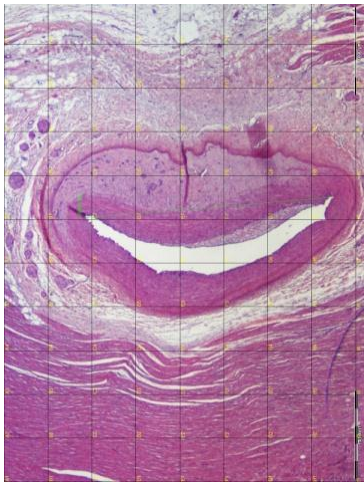


Figure 5. Computer reconstruction and simulation of LAD 15mm after bifurcation and IVUS lumen segmentation (upper panel) and histological analysis (bottom panel)

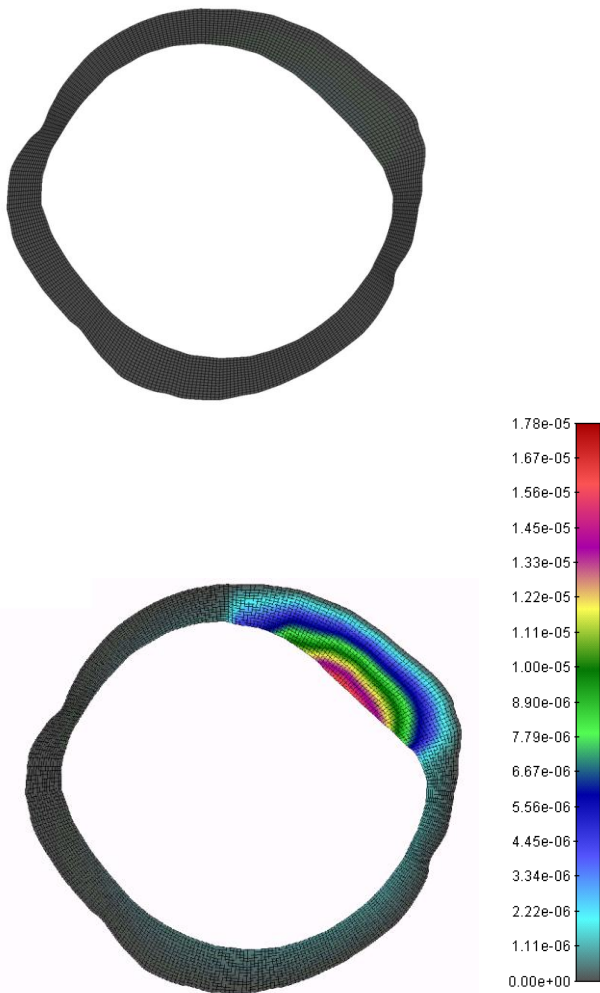


Figure 6. Macrophage concentration [mg/ml] before (upper) and after (bottom) 2 months of the high fat diet on the LAD 15 mm below bifurcation. Red color denotes maximum macrophages concentration.

Comparison of numerical and experimental results for high fat diet pig is presented in Figure 7. It can be seen that numerical and experimental results are very close for lesion area and foam cell lipids. The initiator for plaque formation is shear stress function.

#### 4. Conclusion and Discussion

Full three-dimensional model is created for plaque formation and initial progression, coupled with blood flow and LDL concentration in blood. The Navier-Stokes equations together with the Darcy law for model blood filtration and Kedem-Katchalsky equations for the solute and flux transfer are implemented. Additionally, the system of three additional reaction-diffusion equations for simulation of the inflammatory process is coupled with full incremental iterative procedure. The wall permeability was assumed to be function of wall shear stress with more permeability with low and oscillatory shear stress. Two examples are examined: Cheng example from literature (Cheng et al 2006, [20]) and our own experimental data from LAD artery on pig after 2 months of high fat diet. In Cheng experiment we tried to match plaque composition with macrophages and lipids concentration in the intimal area for two different wall shear stress zones. Parameters are fitted with nonlinear least square procedure. We included the effects of wall shear stress on the wall permeability as well as both volume and solute flux. Although the model is taken into account time and space for atherosclerosis process a lot of parameters and thresholds from our model are still unknown and we assumed their values in the simulation. The concentration values for macrophages and lipids are in good agreement with Cheng experiment.

Our computer model was performed on the pig experiment after 2 months high fat diet. A specific procedure for matching geometrical data from IVUS and histological cross-section was developed. It includes deformation of elastic body from histological initial to IVUS internal wall shape. We should note that the animal model investigated the very early phase of coronary atherosclerosis. A small initial plaque was observed at LAD 15mm after bifurcation which corresponds low shear stress location performed with computational analysis. Even more we match volume plaque progression with 8% from intimal area for specific diet time frame of 2 months. Velocity of plaque progression from eqs 7-9 is firstly fitted and then other simulation parameters. The thresholds for this model are assumed to be zero because there is no measurement of these values in the current literature to our knowledge. Our work is a novel way of modeling plaque formation and development. Matching of plaque location and progression in time between experimental and computer model shows a potential benefit for future prediction of this vascular disease using computer simulation. Further development should investigate influence of the pulsatility flow condition on our model, a proliferation of the smooth muscle cells and

direct values of the threshold parameters which could be obtained from appropriate experiments not available currently.

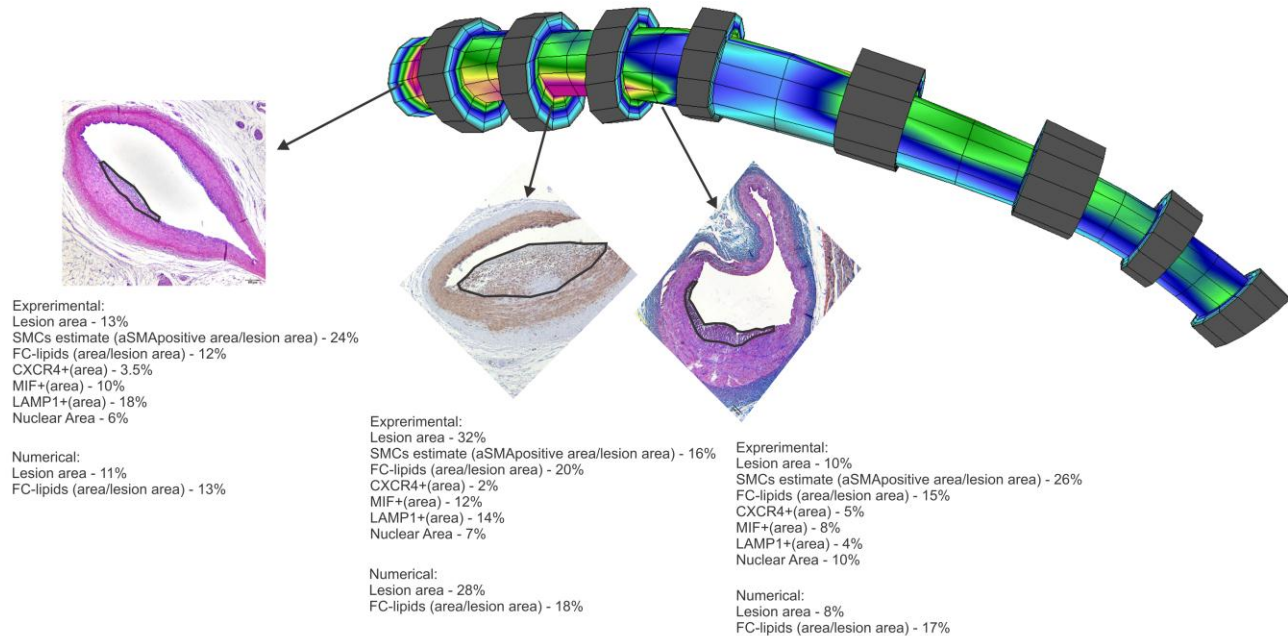


Figure 7. Comparison of experimental and numerical results

## Acknowledgements

This study was funded by a grant from FP7-ICT-2007 project (grant agreement 224297, ARTreat) and grants from Serbian Ministry of Science III41007 and ON174028.

## References

- [1] P. Libby, Inflammation in atherosclerosis. *Nature*, 2002, 868–874.
- [2] J. Loscalzo & A.I. Schafer, *Thrombosis and Hemorrhage* (Third edition. Lippincott Williams & Wilkins, Philadelphia, 2003).
- [3] J.M. Tarbell, Mass transport in arteries and the localization of atherosclerosis, *Annual Review of Biomedical Engineering*, 5, 2003, 79–118.
- [4] P. Zunino, *Mathematical and numerical modeling of mass transfer in the vascular system*. (PhD thesis, Lausanne, Switzerland: EPFL, 2002).
- [5] A. Quarteroni, A. Veneziani, P. Zunino, Mathematical and numerical modeling of the solute dynamics in blood flow and arterial walls, *SIAM Journal of Numerical Analysis*, 39, 2002, 1488–1511.
- [6] M.R. Kaazempur-Mofrad, C.R. Ethier, Mass transport in an anatomically realistic human right coronary artery, *Ann Biomed Eng* 29, 2001, 121–127.
- [7] S. Wada, M. Koujiya, T. Karino, Theoretical study of the effect of local flow disturbances on the concentration of low-density lipoproteins at the luminal surface of end-to-end anastomosed vessels, *Med Biol Eng Comput* 40, 2002, 576–587.
- [8] D. K. Stangeby, C.R. Ethier, Computational analysis of coupled blood-wall arterial LDL transport, *J Biomech Eng-T ASME* 124, 2002, 1–8.
- [9] N. Sun, N.B. Wood, A.D. Hughes, S.A.M. Thom, X.Y. Xu, Fluid-wall modelling of mass transfer in an axisymmetric stenosis: effects of shear dependent transport properties, *Ann Biomed Eng* 34, 2006, 1119–1128.
- [10] L. Ai, K. Vafai, A coupling model for macromolecule transport in a stenosed arterial wall, *Int J. Heat Mass Tran* 49, 2006, 1568–1591.
- [11] U. Olgac, V. Kurtcuoglu, V. Poulidakos, Computational modeling of coupled blood-wall mass transport of LDL: effects of local wall shear stress, *Am J. Physiol Heart Circ Physiol* 294, 2008, 909–919.
- [12] R. Ross, Atherosclerosis: a defense mechanism gone awry, *Am J Pathol.*, 143, 1993, 987–1002.

- [13] O. Kedem, A. Katchalsky, A physical interpretation of the phenomenological coefficients of membrane permeability, *The Journal of General Physiology*, 45, 1961, 143–179.
- [14] O. Kedem, A. Katchalsky, Thermodynamic analysis of the permeability of biological membranes to non-electrolytes, *Biochim. Biophys.* 27, 1958, 229–246.
- [15] M. Kojic, N. Filipovic, B. Stojanovic, N. Kojic, *Computer Modeling in Bioengineering: Theoretical Background, Examples and Software* (John Wiley and Sons, Chichester, England, 2008).
- [16] V. Calvez, E. Abderrahaman, N. Meunier, A. Raoult, Mathematical modelling of the atherosclerotic plaque formation, *ESAIM Proceedings*, 28, 2008, 1-12.
- [17] N. Filipovic, M. Rosic, I. Tanaskovic, Z. Milosevic, D. Nikolic, N. Zdravkovic, A. Peulic, D. Fotiadis, O. Parodi, ARTreat project: Three-dimensional Numerical Simulation of Plaque Formation and Development in the Arteries, *IEEE Trans Inf Technol Biomed.* 2011, PMID: 21937352.
- [18] N. Filipovic, et al, *PAK-Athero, Specialized three-dimensional software for simulation of plaque formation and development inside the arteries*, (University of Kragujevac, 34000 Kragujevac, Serbia, 2010).
- [19] N. Filipovic, S. Mijailovic, A. Tsuda, M. Kojic, 2006. An implicit algorithm within the Arbitrary Lagrangian-Eulerian formulation for solving incompressible fluid flow with large boundary motions, *Comp. Meth. Appl. Mech. Eng.*, 195, 2006, 6347-6361.
- [20] C. Cheng, D. Tempel, V.R. Haperen, A. V. D. Baan, F. Grosveld, M.J.A.P. Daemen, R. Krams, D.R. Crom Atherosclerotic lesion size and vulnerability are determined by patterns of fluid shear stress, *Circulation*, 113, 2006, 2744-2753.